

Shoulder and Elbow Joint Angle Tracking With Inertial Sensors

Mahmoud El-Gohary* and James McNames

Abstract—Wearable inertial systems have recently been used to track human movement in and outside of the laboratory. Continuous monitoring of human movement can provide valuable information relevant to individuals' level of physical activity and functional ability. Traditionally, orientation has been calculated by integrating the angular velocity from gyroscopes. However, a small drift in the measured velocity leads to increasing integration error over time. To compensate that drift, complementary data from accelerometers are normally fused into tracking systems using the Kalman or extended Kalman filter. In this study, we combine kinematic models designed for control of robotic arms with state-space methods to continuously estimate the angles of human shoulder and elbow using two wearable inertial measurement units. We use the unscented Kalman filter to implement the nonlinear state-space inertial tracker. Shoulder and elbow joint angles obtained from 8 subjects using our inertial tracker were compared to the angles obtained from an optical-tracking reference system. On average, there was an RMS angle error of less than 8° for all shoulder and elbow angles. The average correlation coefficient for all movement tasks among all subjects was $r \geq 0.95$. This agreement between our inertial tracker and the optical reference system was obtained for both regular and fast-speed movement of the arm. The same method can be used to track movement of other joints.

Index Terms—Elbow, inertial sensors, joint angle tracking, kinematics, shoulder, wearable devices.

I. INTRODUCTION

MEASUREMENT and analysis of human movement has many applications including diagnosis of neurological movement disorders, rehabilitation from injury, and enhancement of athletic performance. Movements can be measured using a wide variety of techniques and sensors. Optical systems have been widely used to assess leg, elbow, and shoulder kinematics noninvasively. They rely on measurements of reflected or emitted light [1]. Motion is captured by placing reflective markers on the body and cameras are used to record the markers positions. Optical systems are the most common and accurate in tracking movement [2]. However, they require a clear line of sight between the source and the sensor, are costly, and can only be used in a laboratory environment.

Manuscript received May 6, 2012; revised June 26, 2012; accepted July 10, 2012. Date of publication July 13, 2012; date of current version August 16, 2012. Asterisk indicates corresponding author.

*M. El-Gohary is with the Biomedical Signal Processing Laboratory, Department of Electrical and Computer Engineering, Portland State University, Portland OR 97201, USA (e-mail: mahmoud@pdx.edu).

J. McNames (Director) is with the Biomedical Signal Processing Laboratory, Department of Electrical and Computer Engineering, Portland State University, Portland OR 97201, USA (e-mail: mcnames@pdx.edu).

Color versions of one or more of the figures in this paper are available online at <http://ieeexplore.ieee.org>.

Digital Object Identifier 10.1109/TBME.2012.2208750

A typical inertial measurement unit (IMU) is a compact wearable device that contains a triaxial accelerometer and a triaxial gyroscope. Accelerometers measure the translational acceleration and acceleration due to gravity. Gyroscopes measure angular velocities. Wearable inertial sensors are simpler, unobtrusive, and self-contained. They are suitable for continuously monitoring over long periods while the subject performs normal activities of daily life at home. Fig. 2 shows an example of Opal sensor (Ambulatory Parkinsons Disease Monitoring, Inc., Portland, OR) used in this study.

Traditionally, orientation of a segment has been estimated by integrating the angular velocities measured by gyroscopes, and position is obtained by double integration of the translational acceleration measured by accelerometers. A significant problem with integration, however, is that inaccuracies inherent in the measurements quickly accumulate and rapidly degrades accuracy. Roetenberg showed that integration of noisy gyroscope data resulted in a drift of 10° – 25° after 1 min [3].

One approach to reducing integration drift is to fuse the gyroscope data with complementary data from other sensors. Luinge *et al.* estimated orientation of body segments by fusing gyroscope and accelerometer data [4], [5]. The orientation obtained by integrating angular rate was split into tilt and orientation around the global vertical axis. The difference between gyroscope and accelerometer tilt was fused with a Kalman filter to more accurately estimate the tilt. This was then combined with the rotation around the vertical axis to produce a better orientation estimate. However, the estimation was accurate for only brief periods when the subject was not moving and when acceleration was only due to gravity.

To alleviate the cumulative drift around the vertical axis encountered in their earlier system [6], Luinge *et al.* developed a method that used constraints in the elbow to measure the orientation of the forearm with respect to the upper arm [7], [8]. They used one inertial measurement unit near the wrist and another near the elbow. Heading error between the two arm segments was minimized using the knowledge that the elbow joint does not permit abduction/adduction. The filter estimated the orientation in a way that sets the adduction angle to zero. Although they reported an improvement in estimating the orientation, the average orientation error was 20° .

Giansanti *et al.* combined gyroscopes with accelerometers to track position and orientation during three tasks: stand-to-sit, sit-to-stand, and gait initiation [9]. Error in estimation was minimal. However, they restricted the application to simple tasks and limited the measurements to a time duration of 4 s.

In a series of studies, Bachmann *et al.* used accelerometers and magnetometers in a quaternion-based complementary filter to compensate the drift of the orientation produced by

integrating the angular velocity [10], [11]. The system combined a triaxial accelerometer, a triaxial gyroscope and a triaxial magnetometer assembled to produce a sensor module referred to as Magnetic, Angular Rate and Gravity sensor (MARG). In a later study, Bachmann *et al.* investigated the effect of electrical appliances and furniture made of ferromagnetic materials on the accuracy of orientation tracking using MARG systems [12]. They observed errors that ranged from 12° to 16° and stated that these errors can be avoided by maintaining an approximate distance of two feet from the source of disturbance. This limits the success of their tracking system and restricts its use to custom laboratory environment.

Roetenberg *et al.* argued that errors due to magnetic-field disturbance may be compensated by adequate model-based sensor fusion [13]. They developed a Kalman filter that operated on two inputs. The first was the difference between inclination from the accelerometer and gyroscope. The second input was the difference inclination from the magnetometer and gyroscope. The states of the model included the gyroscope bias error, orientation error, and magnetic disturbance. The filter was tested under quasi-static and dynamic conditions with ferromagnetic materials close to the sensor for less than a minute. The results show that the orientation estimates improved significantly when the magnetic interference correction was used. However, the accuracy could decrease if the magnetic disturbance was due to varying sources that are present during longer periods of testing. In a subsequent study, Roetenberg *et al.* combined a body-mounted magnetic system with gyroscopes and accelerometers to track position and orientation using a complementary Kalman filter [14]. Orientation and position were obtained by single and double integration of gyroscope and accelerometer data, respectively. These were then updated with magnetometer data to improve accuracy. The tracker was tested without metals in the vicinity, and errors were expected to grow if ferromagnetic materials were anywhere close to the magnetic system.

Yun *et al.* used MARG modules and a quaternion-based extended Kalman filter (EKF) to track human body motion. A Gauss–Newton iteration method was used to preprocess accelerometer and magnetometer data to produce quaternion input to the EKF [15]. A rotary tilt table with two DOF's was used to assess the performance of the tracker [16], [17]. The pitch angle error was not reported, and an error of 9° in less than 2 s was obtained for the roll angle. In a recent study, Yun *et al.* presented a simplified algorithm for orientation estimation using only accelerometers and magnetic field measurements [18]. Although the system was suitable for tracking slow movements, the gyroscope-free system is not suited for normal or fast movements, resulting in large orientation errors.

In a series of studies by Zhou *et al.* orientations of wrist and elbow were estimated by fusion of the signals from MARG modules mounted on the wrist and elbow joints [19], [20]. They integrated the rotational rate to localize the wrist and elbow, and smoothed the abrupt amplitude changes to reduce overshoot during fast movements. Three subjects performed a set of tasks that lasted 20 s and was repeated three times with a resting period of 30 s in between. The tasks included reaching a target, drinking, lifting the arm, and flexing the elbow while keeping the

shoulder still. They attained a high correlation between position estimates from the inertial tracker and estimates from a reference optical tracking system ≥ 0.91 [21].

In summary, other groups have used accelerometers and magnetometers to compensate for the orientation error that occurs when integrating the angular rate from gyroscopes, but all of these methods were only applicable under limited circumstances. Some groups restricted the application to simple tasks and short tracking periods. In other studies, the estimation was accurate for only brief periods when the acceleration measurements were only due to gravity. Others reported large orientation errors due to magnetic field disturbances.

In this paper, we combine kinematic models designed for control of robotic arms with state-space methods to directly and continuously estimate human joint angles from inertial sensors. We investigate the performance of our unscented Kalman filter (UKF)-based method by first validating our statistical models using synthetic data. We then investigate the performance of our inertial tracking algorithm by comparing the estimated inertial angles to those obtained from an optical reference system during normal and fast movement of eight subjects performing both simple planar and complex arm movement.

II. THEORY

We use an established method of biomechanical modeling based on a sequence of links connected by joints. This type of model could represent any part of the human body. To systematically describe the position and orientation of each pair of consecutive links, a method was proposed by Denavit and Hartenberg in 1955. The method is widely used in the analysis and control of robotic manipulators [22] and has also been successfully applied to characterize human motion [23]. The method is based on characterizing the relationship between links and joints with a (4×4) transformation matrix. This matrix depends on four parameters associated with each link. The first parameter is the link length a_i , which is the distance from the rotation axis Z_i to Z_{i+1} measured along their common normal axis X_i . The second parameter is the link twist α_i , which is the angle from Z_i to Z_{i+1} measured about the X_i -axis. The distance from X_{i-1} to X_i measured along the Z_i -axis is known as the link offset d_i . The fourth parameter is the joint angle θ_i , which is the angle from X_{i-1} to X_i measured about the Z_i -axis. These four parameters are known as the Denavit–Hartenberg (D-H) parameters and will be specified for the shoulder and elbow in the following section. To describe the location and orientation of each link relative to the one next to it, we attach a frame to each link. The convention of attaching reference frames to upper arm and forearm segments was detailed in [23].

A. Shoulder and Elbow Joint Angles

We present a model for shoulder and elbow movement with five degrees of freedom (DOFs). The shoulder and the shoulder girdle make up one of the most complex joint groups of the human body [24]. This complex joint is typically simplified as a ball-and-socket joint with three DOFs. When a joint has n -DOFs, it can be modeled as n joints of one DOF connected with $n - 1$ links of zero length [22]. Fig. 1 shows the arm

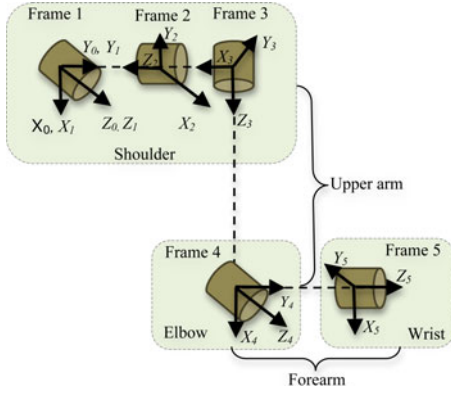


Fig. 1. Kinematics diagram of the arm model with Frame 0 as the static reference frame. Frames 1 through 3 represent shoulder flexion/extension, abduction/adduction and internal/external rotation, respectively. Frames 4 through 5 represent the elbow flexion/extension and forearm pronation/supination.

TABLE I
DENAVIT–HARTENBERG PARAMETERS FOR THE ARM MODEL

Frame	α_{i-1}	a_{i-1}	d_i	θ_i
1	0	0	0	θ_1
2	$\pi/2$	0	0	$\theta_2 + \pi/2$
3	$\pi/2$	0	l_u	$\theta_3 + \pi/2$
4	$\pi/2$	0	0	$\theta_4 + \pi/2$
5	$-\pi/2$	0	l_f	θ_5

model with static base reference frame 0 at the center of the shoulder joint. Frames 1 through 3 represent shoulder flexion/extension, abduction/adduction, and internal/external rotation, respectively. The elbow joint is a hinge joint that allows movement in one plane, flexion/extension, represented by frame 4. The radioulnar joint is a pivot joint that allows for forearm pronation/supination, represented by frame 5 [25].

Table I shows the D-H parameters, where α_{i-1} is the angle to rotate to make the two coordinate systems coincide, l_u is the length of the upper arm, l_f is the length of the forearm, and θ_i is the i th angle of rotation.

B. Propagation of Velocity and Acceleration

To formulate the dynamic equations for the arm IMUs during movement, we use three of the Newton–Euler equations of motion. These forward recursive equations are used to propagate angular velocity, and angular and linear acceleration from the reference coordinate system through the links of upper arm, forearm, and wrist. Each link of the arm in motion has some angular velocity, and angular and linear acceleration ($\omega, \dot{\omega}, \dot{v}$). The velocity ${}^{i+1}\omega_{i+1}$ of link $i+1$ is that of link i plus the new velocity component added by joint $i+1$. Similarly, the angular and linear acceleration of each link are related by the following recursive equations:

$${}^{i+1}\omega_{i+1} = {}^i R^{i+1} \omega_i + \dot{\theta}_{i+1} {}^{i+1} Z_{i+1}$$

$${}^{i+1}\dot{\omega}_{i+1} = {}^i R^{i+1} \dot{\omega}_i + {}^i R^{i+1} \omega_i \times \dot{\theta}_{i+1} {}^{i+1} Z_{i+1} + \ddot{\theta}_{i+1} {}^{i+1} Z_{i+1}$$

$${}^{i+1}\dot{v}_{i+1} = {}^i R^{i+1} [\dot{\omega}_i \times {}^i P_{i+1} + \omega_i \times ({}^i \omega_i \times {}^i P_{i+1}) + \dot{v}_i]$$

where ${}^i R^{i+1}$ is the rotation matrix between the i th and $(i+1)$ th link, \times represents the cross product operation, $\dot{\theta}_i$ is the angular

velocity, ${}^i P_{i+1}$ is the position vector of frame $i+1$, which is the upper-right 3×1 vector of the D-H matrix. The rotation matrices R , can be obtained by taking the transpose of the upper left 3×3 transformation matrix with parameters shown in Table I. Single and double dot notation represents first and second derivatives with respect to time. We initialize $\omega_0 = \dot{\omega}_0 = (0, 0, 0)^T$, and $\dot{v}_0 = (g_x, g_y, g_z)^T$, where g is gravity.

C. State-Space Model

The general discrete time state-space model is of the form

$$x(n+1) = f_n [x(n), u(n)] \quad (1)$$

$$y(n) = h_n [x(n), v(n)] \quad (2)$$

where $x(n)$ is the unobserved state, $y(n)$ is the measured data, $f_n[\cdot]$ and $h_n[\cdot]$ are nonlinear state and observation equations, $u(n)$ and $v(n)$ are the state and observation white noise with zero mean. Our state model equations are given by

$$\theta_i(n+1) = \theta_i(n) + T_s \dot{\theta}_i(n) + \frac{1}{2} T_s^2 \ddot{\theta}_i(n) \quad (3)$$

$$\dot{\theta}_i(n+1) = \dot{\theta}_i(n) + T_s \ddot{\theta}_i(n) \quad (4)$$

$$\ddot{\theta}_i(n+1) = \alpha \ddot{\theta}_i(n) + u_{\ddot{\theta}_i}(n) \quad (5)$$

where $i = \{1, \dots, 5\}$ of the five angles, $\theta_i(n)$ is the i th angle at time n , $\dot{\theta}_i$ is the angular velocity, $\ddot{\theta}_i$ is the angular acceleration, $u_{\ddot{\theta}_i}(n)$ is a white noise process with zero mean, α is a process model parameter, and $T_s = 1/f_s$ is the sampling period. These are standard equations for a physical object moving at a constant acceleration. The model assumes the acceleration is constant for the duration of a sampling interval. This is sufficient for our data, which was acquired with a sample rate of $f_s = 128$ Hz. The angular acceleration is modeled as a first-order autoregressive process with zero mean. Depending on the choice of α , this model ranges from a random walk ($\alpha = 1$) to a white noise model ($\alpha = 0$). For values of $\alpha < 1$ the estimated angular accelerations are biased toward 0, but for human motion this bias is reasonable and may improve performance.

The observation equations were created with an algorithm that algebraically applies the Newton–Euler recursive equations with the parameters in Table I. Equations of the upper arm IMU are

$$\dot{\omega}_z = \dot{\theta}_3 + \dot{\theta}_1 s \theta_2$$

$$\dot{\omega}_x = \dot{\theta}_1 c \theta_2 s \theta_3 - \dot{\theta}_2 c \theta_3$$

$$\dot{\omega}_y = \dot{\theta}_1 c \theta_2 c \theta_3 + \dot{\theta}_2 s \theta_3$$

$$\dot{v}_x = -l_u [\dot{\theta}_1^2 c \theta_2^2 + \dot{\theta}_2^2] - g c \theta_1 c \theta_2$$

$$\dot{v}_y = l_u [c \theta_2 s \theta_2 s \theta_3 \dot{\theta}_1^2 - 2 \dot{\theta}_2 c \theta_3 s \theta_2 \dot{\theta}_1 + \ddot{\theta}_2 s \theta_3 + \ddot{\theta}_1 c \theta_2 c \theta_3] + g [c \theta_3 s \theta_1 + c \theta_1 s \theta_2 s \theta_3]$$

$$\dot{v}_z = l_u [c \theta_2 c \theta_3 s \theta_2 \dot{\theta}_1^2 + 2 \dot{\theta}_2 s \theta_2 s \theta_3 \dot{\theta}_1 + \ddot{\theta}_2 c \theta_3 - \ddot{\theta}_1 c \theta_2 s \theta_3] - g [s \theta_1 s \theta_3 + c \theta_1 c \theta_3 s \theta_2]$$

where $(\omega_x, \omega_y, \omega_z, \dot{v}_x, \dot{v}_y, \dot{v}_z)$ are the gyroscope, and accelerometer data at time n . The time index n was dropped for

ease of readability. Measurement equations for the forearm IMU are too long to be shown in this paper.

D. Nonlinear State Estimator

The state-space arm model introduced earlier has a nonlinear relationship between the joint angles and observed sensor measurements. The EKF is the most common method of nonlinear state estimation. It is based on linearizing the state and observation models with a first-order Taylor series expansion. It models the state variables with first- and second-order moments, which is most appropriate when the distribution is Gaussian. The linearization leads to poor performance if the dynamics are highly nonlinear and the local linearization insufficiently characterizes the relationship. The EKF also requires calculation of Jacobian matrices, which can be difficult, tedious, error prone, and time consuming.

Sequential Monte Carlo methods, which are also known as particle filters, can overcome the performance and implementation limitations of the EKF [26]. These algorithms can be applied to highly nonlinear and non-Gaussian estimation problems, has computational requirements that are orders of magnitude larger than the EKF. While the methods described in this article could be implemented with any of these nonlinear tracking algorithms, in this study we used the UKF [27].

Before the algorithms can be applied, the variance of the measurement noise and the variance of the noise driving the acceleration of the joint angles must be specified. We approximated the measurement noise of the accelerometers and gyroscopes based on short recordings while the sensors were stationary. We used 0.001 and 0.01 for gyroscope and accelerometer noise variance. The variance of the noise driving the acceleration of the joint angles is the primary user-specified tuning parameter. This controls the tradeoff between the smoothness of the estimated angles and how precisely the model tracks the data recorded from the accelerometers and gyroscopes. For all of the results reported here, we used a process noise variance of 1. The joint angle acceleration were modeled as a random walk process ($\alpha = 1$).

E. Performance Assessment

To evaluate the performance of the inertial tracking system, we compared the joint angles calculated by the inertial tracker with those from an optical tracking reference system. We collected two datasets from a total of eight subjects performing tasks described in Table II. The study was conducted in the Balance Disorders Laboratory at Oregon Health and Science University, which is equipped with a motion capture system with eight high-speed, infrared cameras (Motion Analysis Corporation, Santa Rosa, CA). The cameras recorded the position of 14 reflective markers placed on the sternum, upper arm, forearm, shoulder and wrist (see Fig. 2). Elbow and forearm angles were obtained from the 3-D positions of the markers placed on the upper arm and forearm based on the algorithm described in [28]. Similarly, shoulder angles were obtained from positions of the reflective markers placed on the shoulder and upper arm. Two IMUs, containing a triaxial accelerometer and gyroscope, were placed on the upper arm and forearm. Each IMU was attached

TABLE II
AVERAGE CORRELATION r , RMSE, AND PEAK-TO-PEAK ERROR BETWEEN OPTICAL AND INERTIAL ANGLES OF SHOULDER AND ELBOW

Task	r	RMSE($^{\circ}$)	Peak Error($^{\circ}$)
Elbow Flexion/Extension	0.98	6.5	9.8
Forearm Supination/Pronation	0.95	5.5	7.8
Shoulder Flexion/Extension	0.98	5.5	7.9
Shoulder Abduction/Adduction	0.99	4.4	8.1



Fig. 2. Reflective markers and Opal inertial sensors (APDM, Inc.) placement on the arm of one of the subjects.

to the arm with a strap band, in the center of a cluster of four markers. A stationary calibration period of 3 s at the initial pose preceded each movement task. The calibration period served two purposes. The first was to align the inertial and optical reference systems. The second was to calculate the gyroscope constant bias. This bias was removed from the gyroscope data before calculating the joint angles. Optical and inertial systems were synchronized to start and stop recording simultaneously. The inertial data was originally sampled at 128 Hz, and the Vicon data at 60 Hz. The angles calculated from inertial sensors were then resampled to 60 Hz for comparison to the Vicon optical angles.

III. RESULTS

To validate our statistical models, used to generate the state and observation equations, we first investigate the performance of the UKF-based tracker on synthetic data generated by these statistical models. On average, the root-mean-squared error (RMSE) between the synthetic and estimated angles and was less than 0.6° for all five arm angles. Fig. 3 shows the true (solid lines) and estimated (dotted lines) synthetic shoulder angles, and the very small-tracking error in bold gray line.

In the rest of this section, we present results for tracking real data using the inertial and optical systems. In the first dataset, four subjects repeated simple planar articulations three times. Each time lasted 18 s, including a stationary calibration period of 3 s at initial pose. The subjects performed each task at a normal daily life movement speed, at an approximate average of $180^{\circ}/s$, while keeping the rest of the body stationary. Fig. 4 shows forearm supination/pronation angles, and Fig. 5 shows shoulder abduction/adduction angles estimated by the inertial and optical

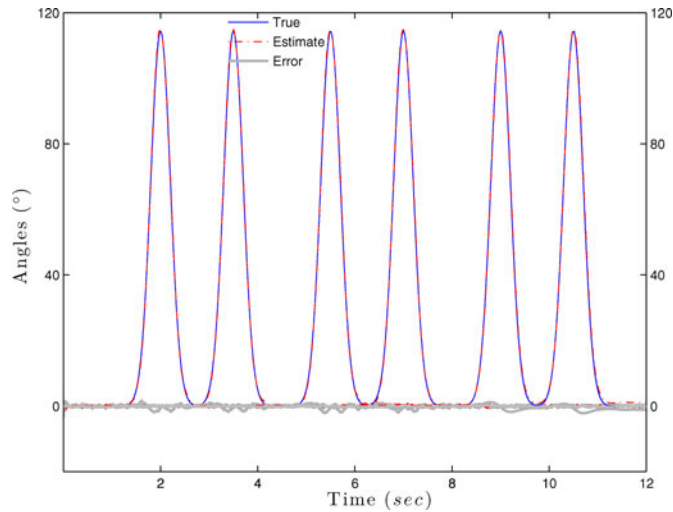


Fig. 3. Synthetic shoulder angles (solid lines), their estimate (dashed), and error (grey). The first two bumps represent flexion/extension. The third and fourth are shoulder abduction/adduction. The last two are internal/external rotation.

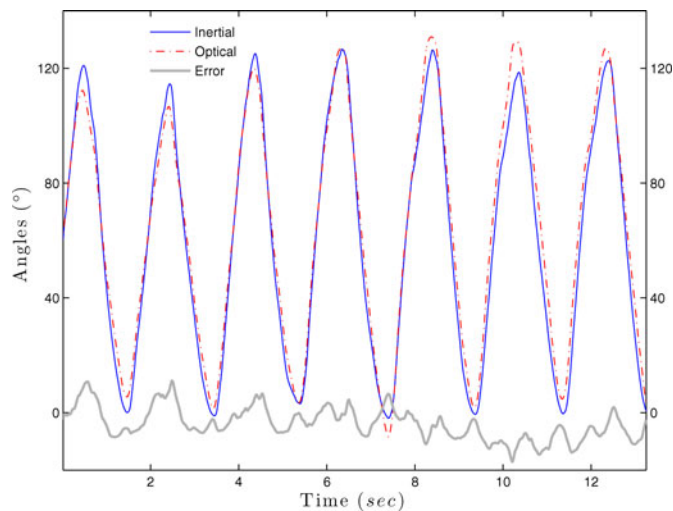


Fig. 4. Forearm supination/pronation estimates by the optical system (dashed line) compared to inertial angles estimate (solid line), and the error in gray.

tracking systems, and the difference between estimates in gray lines.

We calculated the correlation coefficient r , and the RMSE between angle estimates from the inertial and optical tracking system. On average, the correlation coefficient was $r \geq 0.97$ for all tasks among all subjects. Table II shows the correlation coefficient, RMSE average across subjects for all tasks, and the peak-to-peak error between inertial and optical angles.

In the second dataset, the other four subjects performed the same tasks described earlier continuously without stopping the recording. Starting with simple planar articulation, and ending with free movement to mimic touching the nose with the index finger, and reaching for a doorknob. The continuous recording lasted approximately 2 min for each subject. Fig. 6 shows an example of shoulder flexion/extension angles estimated by the

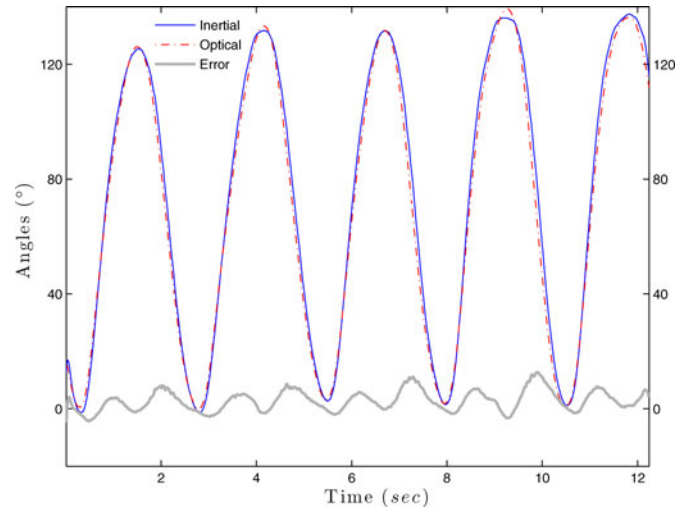


Fig. 5. Shoulder abduction/adduction angle estimates by the optical system (dashed line) compared to inertial angles estimate (solid line), and the error in gray.

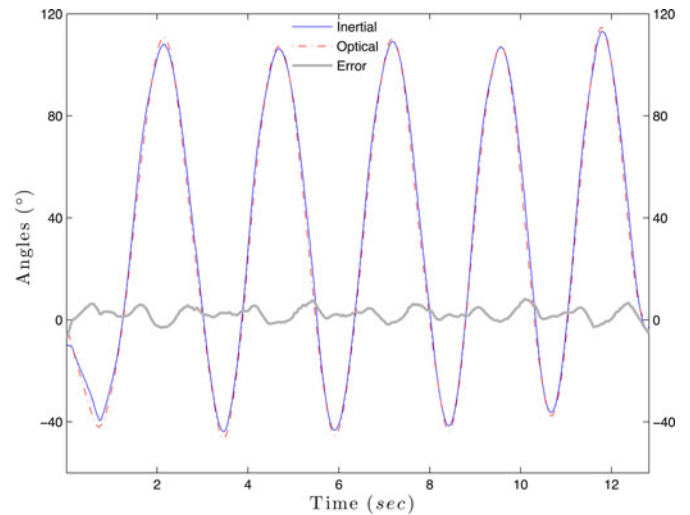


Fig. 6. Shoulder flexion/extension estimates by the optical system (dashed line) compared to inertial angles estimate (solid line), and the error in gray.

inertial and optical tracking systems. The average RMSE for all tasks among the four subjects was less than 7° .

To determine the performance of the inertial tracker when subjects performed more complex movements than simple articulation around one axis, each subject was asked to mimic touching nose with the index finger, and to mimic reaching for the doorknob to open a door. Each movement was repeated five times, lasting about 10s. Both tasks were performed around the end of second minute of recording. Table III shows the average correlation coefficient r among subjects for each task, RMSE, and the peak-to-peak error between inertial and optical angles.

To verify the performance of our inertial system in tracking fast movement, we asked the eight subjects to perform the tasks described in Table II at a fast pace. The articulation was performed at an approximate average rate of $420^\circ/\text{s}$. Fig. 7 shows the estimated inertial elbow flexion/extension angles compared to the angles obtained from the optical system. Average RMSE

TABLE III
AVERAGE CORRELATION r AND RMSE BETWEEN OPTICAL AND INERTIAL
ANGLES OF SHOULDER AND ELBOW

Task	r	RMSE($^{\circ}$)	Peak Error($^{\circ}$)
Touching nose	0.94	6.5	9.8
Reaching for a doorknob	0.95	5.5	8.8

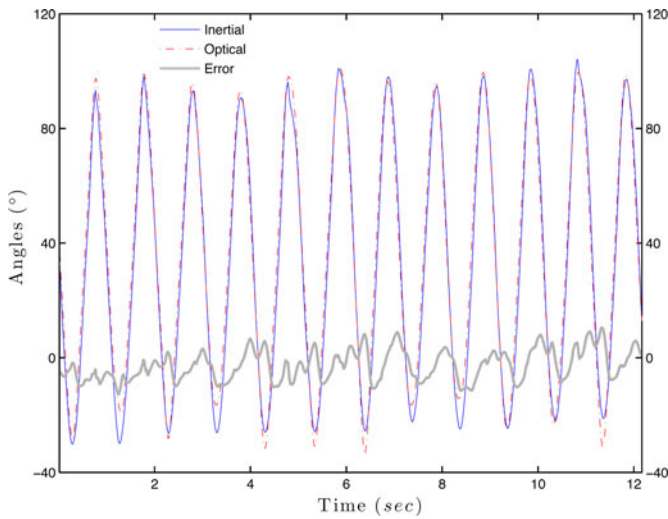


Fig. 7. Elbow flexion/extension during fast arm movement. Inertial estimates (solid line) compared to estimates from the optical system (dashed line).

among the eight subjects for all tasks was less than 8° , and the average peak-to-peak error was less than 12° .

IV. DISCUSSION

We combined kinematic models with state-space methods to estimate human joint angles using IMUs containing a triaxial accelerometer and a triaxial gyroscope. To estimate shoulder and elbow joint angles, we used the UKF which provides a few advantages over the most commonly used EKF. The UKF uses a more accurate method to characterize the propagation of the state variable distribution through the nonlinear models, and it does not require the calculation of Jacobian matrices. In some applications, including the one presented in this study, the calculation of the Jacobian matrices is tedious and error prone due to the structure and dimension of the process and measurement equations.

We compared joint angles estimated by the inertial system to those estimated by an optical tracking reference system. Two different datasets from a total of eight subjects were used to evaluate the performance. In the first dataset, each subject performed 15 s of shoulder and elbow planar articulations at a daily life movement speed with an approximate average rotation rate of $180^{\circ}/s$. RMS angle error between the two systems ranged from 4.4° to 6.5° , with a correlation coefficient $r \geq 0.97$. This is a very reasonable error range compared to what was achieved by Bachmann *et al.* who reported error range of 12° – 16° [12]. Based on the recursive measurement equations, distal segment angles are affected by the accuracy of proximal segments. In other words, error in shoulder angles might result in added error

in elbow angles. Table II shows that maximum estimation error occurred at elbow angles.

The majority of tracking algorithms discussed in the introduction limit their performance assessment to slow movement. We evaluated the performance of our inertial algorithm in tracking fast movement of the eight subjects. Each subject performed the same planar movement at a fast pace, with an approximate average rotation rate of $420^{\circ}/s$. On average, we obtained an RMS angle error of less than 8° for shoulder and elbow angles, with an excellent average correlation coefficient $r \geq 0.95$. During all movement tasks, subjects were instructed to keep the trunk fixed without moving. If the trunk moves, the shoulder and elbow angles will be underestimated or overestimated.

Although errors between optical and inertial angle estimates are minimal, performance is reduced by the noise, bias, and drift of MEMS inertial sensors. Bias generally consists of two parts: a deterministic part called bias offset and a random part. The bias offset refers to the offset in the measurement provided by the inertial sensor, is deterministic in nature. Gyroscope bias offset was determined from a 3-s calibration period of stationary movement at the initial pose. This offset was removed from the gyroscope data before calculating the joint angles. The random drift refers to the rate at which the error in an inertial sensor accumulates with time. Gyroscope and accelerometer random drift can be modeled as a stochastic process; increasing the dimension of the process model by adding six more states for each IMU.

Some of the estimation errors might also be attributed to markers moving independently of each other, especially during fast movements. Fig. 7 shows that maximum errors occurred when the elbow reached its peak flexion or extension. Marker placement over anatomical landmarks can create skin artifacts. The motion of the skin-mounted markers are usually greater than bone markers [29]. Soft-tissue artifact is caused by the relative displacement of markers mounted on the skin surface, and is a major source of error in the kinematic measurement of human movement. Another common problem in motion capture is marker occlusion. When a significant proportion of markers data was missing in any of the recordings, the recording had to be discarded. Six of 56 recordings were discarded due to missing marker data. Vicon data was sampled at 60 Hz. When one or two markers were nonvisible for six frames or less, the occluded marker positions were estimated from neighboring markers using interpolation.

An excellent agreement was also maintained between inertial and optical angle estimates during target reaching and touching nose with the index finger. Table III shows an average RMSE among all subjects that is less than 7° , and an average peak-to-peak error less than 10° .

Because the state-space model includes both the translational and gravitational components of acceleration, the algorithm is accurate during both fast and slow movements. However, one of the limitations of this study, and of all of tracking algorithms discussed in the introduction, is the use of short periods of movement for performance assessment. Although, we used longer periods than most of other studies, our continuous recordings lasted only 2 min for four of the eight subjects. To mitigate the effect of sensors drift on the estimated angles during longer

periods of movement, we plan to use a modified state model. The model will incorporate prior knowledge of physical constraints and human natural range of motion, as well as the gyroscope and accelerometer random drift. The combined effect of imposing physical constraints on state estimates and modeling the sensor random drift are expected to result in better joint angle estimates by our tracking system which does not utilize magnetometer measurements. This could eliminate the need to using magnetic sensors in other systems, which leads to large errors due to magnetic field disturbances [12]. We also plan to compare the performance of the EKF to that of the UKF in estimating the joint angles, given the nonlinear relationship between the joint angles and the observed sensor measurements.

V. CONCLUSION

We combined kinematic models designed for control of robotic arms with state-space methods to directly and continuously estimate human shoulder and elbow joint angles using wearable inertial sensors containing a triaxial accelerometer and gyroscope. These algorithms can be applied to any combination of synchronized sensors and can be generalized to track any limb movement. The implementation can use tracking algorithms that are either causal, real-time or non-causal, offline smoothing with higher accuracy. The agreement between our inertial tracker and a traditional optical motion capture reference system was excellent. This agreement was obtained for both regular and fast speed, and for simple planar and more complex movement of the arm. However, unlike optical systems which require fixed cameras in a controlled environment and suffer from problems of occlusion, wearable inertial sensors can be used anywhere, cannot be occluded, and are low cost. They are suitable for continuous monitoring over long periods while the subject performs normal activities of daily life at home.

ACKNOWLEDGMENT

J. McNames and Portland State University (PSU), Portland, OR, have a significant financial interest in Ambulatory Parkinsons Disease Monitoring, Inc., Portland, OR, a company that may have a commercial interest in the results of this research and technology. The potential individual and institutional conflicts of interest have been reviewed and managed by PSU.

REFERENCES

- [1] G. Welch and E. Foxlin, "Motion tracking: No silver bullet, but a respectable arsenal," *IEEE Comput. Graphics Appl.*, vol. 22, no. 6, pp. 24–38, Nov/Dec. 2002.
- [2] N. L. Keijsers, M. W. Horstink, and S. C. Gielen, "Online monitoring of dyskinesia in patients with Parkinson's disease," *IEEE Eng. Med. Biol. Mag.*, vol. 22, no. 3, pp. 96–103, May/June. 2003.
- [3] D. Roetenberg, "Inertial and magnetic sensing of human motion," Ph.D. dissertation, University of Twente, Enschede, The Netherlands, 2006.
- [4] H. J. Luinge, P. H. Veltink, and C. T. M. Baten, "Estimating orientation with gyroscopes and accelerometers," *Technol. Health Care*, vol. 7, no. 6, pp. 455–459, Jan. 1999.
- [5] H. J. Luinge, "Inertial sensing of human motion," Ph.D. dissertation, University of Twente, Enschede, The Netherlands, Dec. 2002.
- [6] H. J. Luinge and P. H. Veltink, "Measuring orientation of human body segments using miniature gyroscopes and accelerometers," *Med. Biol. Eng. Comput.*, vol. 43, no. 2, pp. 273–282, Mar. 2005.
- [7] H. J. Luinge, P. H. Veltink, and C. T. M. Baten, "Ambulatory measurement of arm orientation," *J. Biomechanics*, vol. 40, pp. 78–85, 2007.
- [8] H. J. Luinge, D. Roetenberg, and P. J. Slycke, "Motion tracking system," U.S. Patent 2008/0285805 A1, Nov. 2008.
- [9] D. Giansanti, G. Maccioni, and V. Macellari, "The development and test of a device for the reconstruction of 3-D position and orientation by means of a kinematic sensor assembly with rate gyroscopes and accelerometers," *IEEE Trans. Biomed. Eng.*, vol. 52, no. 7, pp. 1271–1277, Jul. 2005.
- [10] E. R. Bachmann, "Inertial and magnetic tracking of limb segment orientation for inserting humans in synthetic environments," Ph.D. dissertation, Naval Postgraduate School, Monterey, CA, 2000.
- [11] E. R. Bachmann and R. B. McGhee, "Inertial and magnetic posture tracking for inserting humans into networked virtual environments," in *Proc. ACM Symp. Virtual Reality Softw. Technol.* New York, NY: ACM, 2001, pp. 9–16.
- [12] E. R. Bachmann, X. Yun, and C. Peterson, "An investigation of the effects of magnetic variations on Inertial/Magnetic orientation sensors," in *Proc. IEEE Int. Conf. Robot. Autom.*, 2004, pp. 1115–1122.
- [13] D. Roetenberg, H. J. Luinge, C. T. M. Baten, and P. H. Veltink, "Compensation of magnetic disturbances improves inertial and magnetic sensing of human body segment orientation," *IEEE Trans. Neural Syst. Rehabil. Eng.*, vol. 13, no. 3, pp. 395–405, Sep. 2005.
- [14] D. Roetenberg, P. J. Slycke, and P. H. Veltink, "Ambulatory position and orientation tracking fusing magnetic and inertial sensing," *IEEE Trans. Biomed. Eng.*, vol. 54, no. 5, pp. 883–890, May 2007.
- [15] X. Yun, M. Lizarraga, E. R. Bachmann, and R. B. McGhee, "An improved quaternion-based Kalman filter for real-time tracking rigid body orientation," in *Proc. IEEE/RSJ Int. Conf. Robot. Syst.*, 2003, vol. 2, pp. 27–31.
- [16] X. Yun, C. Aparicio, E. R. Bachmann, and R. B. McGhee, "Implementation and experimental results of a quaternion-based Kalman filter for human body motion tracking," in *Proc. IEEE Int. Conf. Robot. Autom.*, 2005, pp. 317–322.
- [17] X. Yun and E. R. Bachmann, "Design, implementation, and experimental results of a quaternion-based Kalman filter for human body motion tracking," *IEEE Trans. Robot.*, vol. 22, pp. 1217–1227, 2006.
- [18] X. Yun, E. R. Bachmann, and R. B. McGhee, "A simplified quaternion-based algorithm for orientation estimation from earth gravity and magnetic field measurements," *IEEE Trans. Instrum. Meas.*, vol. 57, no. 3, pp. 638–650, 2008.
- [19] H. Zhou and H. Hu, "Inertial motion tracking of human arm movements in stroke rehabilitation," in *Proc. IEEE Int. Conf. Mechatronics Autom.*, 2005, pp. 1306–1311.
- [20] H. Zhou, H. Hu, and Y. Tao, "Inertial measurements of upper limb motion," *Med. Biological Eng. Comput.*, vol. 44, pp. 479–487, 2006.
- [21] H. Zhou and H. Hu, "Upper limb motion estimation from inertial measurements," *Int. J. Inf. Technol.*, vol. 13, no. 1, pp. 1–14, 2007.
- [22] J. J. Craig, *Introduction to Robotics, Mechanics and Control*, (Electrical and Computer Engineering: Control Engineering Series). Boston, MA: Addison-Wesley, 1989.
- [23] M. El-Gohary, L. Holmstrom, J. Huisinga, E. King, and J. McNames, "Upper limb joint angle tracking with inertial sensors," in *Proc. IEEE Ann. Int. Conf. Eng. Med. Biol. Soc.*, 2011, pp. 5629–5632.
- [24] J. L. Pons, R. Ceres, and L. Calderon, *Wearable Robots: Biomechanical Exoskeletons*, J. L. Pons, Ed., 2nd ed. Hoboken, NJ: Wiley, 2008.
- [25] J. Hamill and K. M. Knutzen, *Biomechanical Basis of Human Movement*, P. Darcy, Ed., 2nd ed. Baltimore, MD: Lippincott Williams & Wilkins, 2003.
- [26] O. Cappé, S. Godsill, and E. Moulines, "An overview of existing methods and recent advances in sequential monte carlo," *Proc. IEEE*, vol. 95, no. 5, pp. 899–924, May 2007.
- [27] S. J. Julier and J. K. Uhlmann, "Unscented filtering and nonlinear estimation," *Proc. IEEE*, vol. 92, Mar. 2004, pp. 401–422.
- [28] E. S. Grood and W. J. Suntay, "A joint coordinate system for the clinical description of three-dimensional motions: Application to the knee," *American Soc. Mechanical Eng.*, vol. 105, pp. 136–142, 1983.
- [29] A. G. Cutti, C. Troncossi, A. Davalli, and R. Sacchetti, "Soft tissue artefact assessment in humeral axial rotation," *Gait Posture*, vol. 21, pp. 341–349, 2005.

Authors' photographs and biographies not available at the time of publication.